Multimodal, multiphoton microscopy and image correlation analysis for characterizing corneal thermal damage

Wen Lo*
National Taiwan University
Taipei, Taiwan
and
National Cheng Kung University
Department of Engineering Science
Tainan, Taiwan

Yu-Lin Chang*
Jia-Shiu Liu
Chiu-Mei Hseuh
Vladimir Hovhannisyan
National Taiwan University
Department of Physics
and
Center for Quantum Science and Engineering
Taipei, Taiwan

Shean-Jen Chen
National Cheng Kung University
Department of Engineering Science
Tainan, Taiwan

Hsin-Yuan Tan
Chang Gung University
College of Medicine
Chang Gung Memorial Hospital
Department of Ophthalmology
Tao Yuan 333, Taiwan
and
National Taiwan University
College of Medicine
and
College of Engineering
Institute of Biomedical Engineering
Taipei, Taiwan

Chen-Yuan Dong
National Taiwan University
Department of Physics
and
Center for Quantum Science and Engineering
Taipei, Taiwan

Abstract. We used the combination of multiphoton autofluorescence (MAF), forward second-harmonic generation (FWSHG), and backward second-harmonic generation (BWSHG) imaging for the qualitative and quantitative characterization of thermal damage of *ex vivo* bovine cornea. We attempt to characterize the structural alterations by qualitative MAF, FWSHG, and BWSHG imaging in the temperature range of 37 to 90°C. In addition to measuring the absolute changes in the three types of signals at the stromal surface, we also performed image correlation analysis between FWSHG and BWSHG and demonstrate that with increasing thermal damage, image correlation between FWSHG and BWSHG significantly increases. Our results show that while MAF and BWSHG intensities may be used as preliminary indicators of the extent of corneal thermal damage, the most sensitive measures are provided by the decay in FWSHG intensity and the convergence of FWSHG and BWSHG images. [DOI: 10.1117/1.3213602]

Keywords: second-harmonic generation (SHG); autofluorescence (AF); cornea; thermal damage.

Paper 08221R received Jul. 9, 2008; revised manuscript received Apr. 22, 2009; accepted for publication Jul. 6, 2009; published online Oct. 1, 2009.

1 Introduction

Since the realization that nonlinear optical signals of second-harmonic generation (SHG) and multiphoton excited fluorescence (MEF) may be effectively applied for biomedical imaging, optical microscopy entered a new realm of in-depth tissue imaging.[1] Among the well-known advantages of multiphoton microscopy, enhanced imaging depth, confocal-like imaging quality, and increased specimen longevity enabled this approach to become the preferred choice for many tissue imaging applications. A number of pathological conditions such as skin aging,[2] basal cell carcinoma,[3,4] and melanoma[5] have been demonstrated to be distinguishable from the normal tissue states.

*These authors contributed equally to this work.
Address all correspondence to: Hsing-Yuan Tan, Department of Ophthalmology, Chang Gung Memorial Hospital, Linko 333, Taiwan, E-mail: b0401018@adm.cgmh.org.tw; Chen-Yuan Dong, Department of Physics, National Taiwan University, Taipei 106, Taiwan, E-mail: cydong@phys.ntu.edu.tw

1083-3668/2009/14(5)/054003/6/$25.00

In recent years, one particular tissue that has attracted considerable attention is the cornea. As the main refractive element in human vision, corneal health is closely related to the quality of vision. However, since a cornea is approximately 94% transmitting in the visible range, it has been difficult to study this organ with traditional one-photon imaging modalities. While reflected confocal microscopy has been effective in imaging the corneal epithelium and keratocytes,[6–10] corneal stroma composed almost entirely of type I collagen remains virtually invisible to reflected confocal imaging. However, since fibrous collagen are not centrally symmetric in structure, the nonvanishing second-order susceptibility tensor χ_{ijk} can contribute to SHG from the polarization (P_i) effect induced by the external electric field E:

$$P_i = \chi_{ij}E_j + \chi_{ijk}E_jE_k + \chi_{ijkl}E_jE_kE_l + \ldots . \quad (1)$$

Therefore, since corneal stroma is composed largely of type I collagen, one can expect that SHG imaging would be an effective tool for imaging physiological and pathological conditions of the cornea.[11–15]

In previous studies, multiphoton autofluorescence (MAF) and SHG imaging have been effectively applied for corneal imaging. Structurally, MAF was effective in imaging corneal epithelia, while SHG microscopy can be used for characterizing corneal stroma.[16–19] Furthermore, pathological conditions such as corneal thermal damage, keratoconus, infectious keratitis, corneal scar, and corneal wound have been shown to be distinguishable from the normal tissue by multiphoton imaging.[11–14,18,20–22] Among these studies, a feature that is of particular interest is the difference of the forward SHG (FWSHG) and backward SHG (BWSHG) in the imaging of the ocular surface. While FWSHG and BWSHG images of the sclera reveal similarity in the structures of the fibrous collagen matrix, BWSHG of the transparent cornea is distinctively different from the FWSHG results and is not effective in revealing the fibrous architecture of the corneal stroma.[23,24] A reasonable explanation for this phenomenon is that in turbid tissues, both the intrinsic BWSHG and the backscattered FWSHG contribute to backward-detected signals. However, the high transparency of cornea greatly reduces backscattered FWSHG signals, and it is conceivable that interference between adjacent and orthogonal layers contributed to the different morphological features of transparent corneas in the FWSHG and BWSHG images.

Recently, there have been reports using BWSHG for the imaging and quantitative determination of the extent of collagen thermal damage, including that of the porcine stroma.[14,25–28] It was found that at sufficiently high temperatures, BWSHG decreases. However, since the BWSHG and FWSHG images of the normal cornea are morphologically different, it is natural to ask whether BWSHG can be used for the accurate characterization of corneal thermal damage. In addition to decreasing BWSHG, previously reports show that an increase in autofluorescence (AF) intensity accompanies collagen thermal damage and that such increase may be due to tyrosine dimerization.[29–31] In this work, we used a multimodal imaging approach (MAF, BWSHG, and FWSHG) for the imaging and quantification of corneal thermal damage. In addition to determining the temperature dependence of the MAF, BWSHG, and FWSHG signals, we computed the image correlation index (ICI) at different temperatures, which provides quantification of morphological similarity between BWSHG and FWSHG images. From these analyses, we attempt to identify quantitative parameters useful for characterizing the extent of corneal thermal damage.

2 Materials and Methods

2.1 *Multiphoton Instrumentation*

For comparison with earlier research of corneal thermal damage on porcine eyeball, the entire bovine eyeball is placed on an inverted microscope for BWSHG imaging after thermal treatment. Afterward, the central cornea is excised and place on an upright, multimodal multiphoton microscope for MAF, BWSHG, and FWSHG imaging.

The multiphoton imaging system we used was based on a diode-pumped solid-state (Millennia X, Spectra Physics, Mountain View, California) pumped femtosecond, titanium-sapphire laser (Tsunami, Spectra Physics) operating at the excitation wavelength of 780 nm. After passing through the beam controlling optics, the laser source is guided into an upright (E800, Nikon, Japan) or inverted (TE2000, Nikon) microscope, beam-expanded, and reflected into the focusing objectives (upright microscope: Fluor, WI, 40×, NA 0.8, Nikon; inverted microscope: XLUMPLFL20XW, NA 0.95, Olympus) by a main dichroic mirror (700 dcspruv-3p, Chroma Technology, Rockingham, Vermont). Using an x-y galvanometer set, the focused excitation spot is directed onto different positions of the specimen. Powers of 73 mW (at specimen) and 100 mW were used on the corneal button and the entire eyeball, respectively.

In each optical scan using the upright system, a 256×256 pixelated region covering an area 55×55 μm^2 is scanned in 1.3 s. In the inverted microscope, each 512×512 pixelated image with actual size 101×101 μm^2 is acquired within 5.2 s. For large area imaging, after each optical scan, the specimens are translated by a sample positioning stage (H101, Prior ScientificInstruments Ltd., Cambridge, UK) In this manner, a large-area image 400×400 μm^2 in size was obtained in the upright system, and the corresponding image size of 500×500 μm^2 was achieved in the inverted system. The multiphoton images were obtained at the stromal surface.

In both the intact eyeball and excised corneal button imaging, MAF and BWSHG is collected in the epi-illuminated geometry by the focusing objective, and the collected signals first pass through the short-pass, main dichroic mirror. In the upright, multimodal system, the broadband MAF and BWSHG signal are then separated by a secondary dichroic mirror (435 dcxr, Chroma Technology) and respectively filtered by two bandpass filters (MAF: E4351p–700sp, BWSHG: HQ390/20, Chroma Technology) before reaching the detectors. Photon-counting photomultiplier tubes (R7400P, Hamamatsu, Japan) were used in the detection of MAF (435 to 700 nm) and BWSHG (380 to 400 nm) signals. On the other hand, the FWSHG signal was collected by a lens (focal length: 100 mm), reflected by a dichroic mirror (435 dcxr, Chroma Technology), and filtered by a bandpass filter (HQ390/20, Chroma Technology) before reaching the photon-counting photomultiplier (R5700P, Hamamatsu, Japan) for detection. In the inverted system, the BWSHG signals are fil-

tered by a series of sequentially aligned dichroic mirrors (555 dcxr, 460 dcxr, and 435 dcxr, Chroma Technology) and a bandpass filter (HQ390/20, Chroma Technology).

2.2 *Corneal Specimens and Thermal Treatment*

To obtain the bovine corneas used in this study, fresh bovine eyeballs are obtained from a local meat shop. Entire bovine eyeballs were heated in PBS buffer at 13 temperatures of 37, 40, 45, 50, 53, 55, 60, 65, 70, 75, 80, 85 and 90°C for 10 min. After thermal treatment, the eyeballs are de-epithelialized and mounted on an inverted multiphoton microscope to obtain epi-luminescent BWSHG. After that, the central corneal button with 7 mm in diameter is excised for the acquisition of broadband MAF, BWSHG, and FWSHG using our upright, multiphoton multimodal system. For statistical significance, two randomly selected regions in each eyeball and three eyeballs at each temperature were imaged. As a result, six multiphoton images at each temperature were acquired and analyzed.

2.3 *Imaging Analysis*

To compare with the results in our earlier publication,[14] the BWSHG signals obtained from entire eyeballs are computed over a $500 \times 500\ \mu m^2$ area. Intensities of the MAF, FWSHG, and BWSHG signals in corneal buttons were computed over the large imaged area of $400 \times 400\ \mu m^2$. In addition, the similarity between FWSHG and BWSHG images was determined through the image correlation index (ICI) based on Pearson's product-moment coefficient. In this definition, ICI is given as:

$$\sum_i \frac{(I_{FWSHG,i} - \mu_{FWSHG}) \cdot (I_{BWSHG,i} - \mu_{BWSHG})}{\sigma_{FWSHG} \cdot \sigma_{BWSHG}}, \qquad (2)$$

where I is the respective signal intensity at pixel i. Furthermore, μ and σ represent the average intensity and standard deviation of the entire image, respectively. In analyzing the correlation between the BWSHG and FWSHG images, image correlation is computed over the entire imaged area. For two images that are morphologically identical, the ICI is one, and two uncorrelated images would yield an ICI value of zero.

3 Results

Shown in Fig. 1 are the FWSHG and BWSHG images of untreated bovine cornea at the stromal surface. In the magnified images in Fig. 1(c) and 1(d), fibril-like structure can be observed in both FWSHG and BWSHG images, as the white dashed lines indicate. However, while FWSHG effectively outlines the fibrous architecture of type I collagen matrix in stroma, the BWSHG image lacks the clear outline of the fibrous structure of the FWSHG results. To quantify morphological similarity between the images, we calculated the ICI between the FWSHG and BWSHG images and found a value of 0.35.

The intensity profile of corneal BWSHG obtained from entire bovine eyeballs are shown in Fig. 2. Our results show the general trend that BWSHG from corneas on intact eyeballs increases as the treating temperature rises and then decreases at higher temperature. Specifically, the BWSHG intensity increased from 37 to 40°C. In addition, local intensity

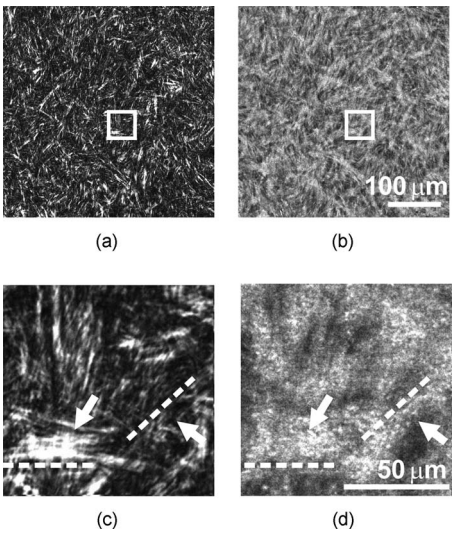

Fig. 1 FWSHG and BWSHG images observed on the stromal surface of a normal bovine corneal button are shown in Figs. 1(a) and 1(b), respectively, while selected regions of interest in Figs. 1(a) and 1(b) are magnified and shown in Fig. 1(c) and 1(d), respectively.

maxima at 55, 65, and 80°C were found. These results compare favorably to the results of the previous study,[14] where BWSHG increases dramatically when the temperature was raised to 45°C with additional intensity peaks at 53, 65, and 78°C. However, unlike the previous study, the temperature dependence of the BWSHG intensity in the current study did not decay significantly at temperatures above 80°C. This difference may be due to the different degree of collagen cross-linking between the bovine and porcine corneas.

In addition to BWSHG intensity analysis from intact eyeballs, we also compared and analyzed the FWSHG and BWSHG images of the thermally treated bovine cornea buttons at stromal surface. In particular, representative images at the treatment temperatures of 37, 53, 60, 75, and 85°C are shown in Fig. 3. At the two lower temperatures of 37 and 53°C, BWSHG and FWSHG images show morphologically distinct features, with the FWSHG images clearly delineating the fibrous architecture of stromal collagen. However, our results show that 60°C is the threshold temperature for the appear-

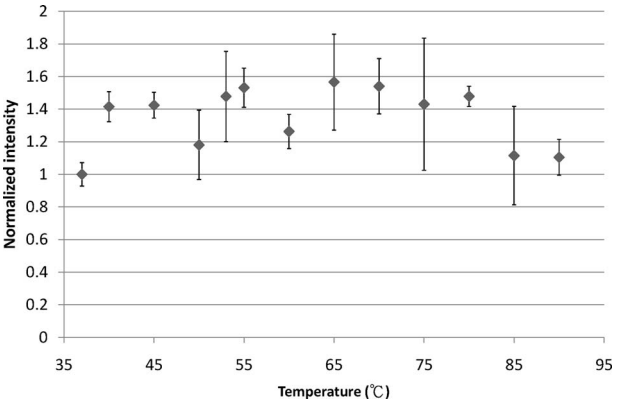

Fig. 2 Temperature dependence of BWSHG intensity of bovine corneas (intact eyeballs).

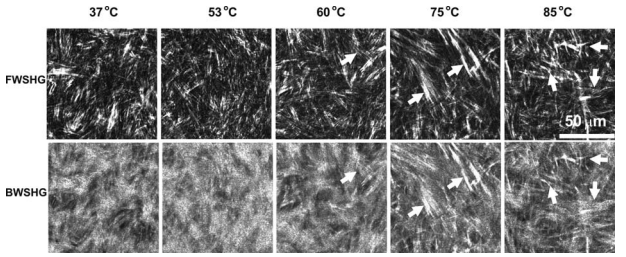

Fig. 3 Representative FWSHG and BWSHG images of bovine corneas at the treatment temperatures of 37, 53, 60, 75 and 85°C. White arrows indicate distinct fibrous structures in BWSHG images and the corresponding locations in FWSHG images.

ance of fibrous structure in BWSHG. When the temperature rises over 60°C, distinguishable fibers can be observed in BWSHG images. At the higher temperatures of 75 and 85°C, the fibrous nature of individual collagen fibers becomes increasingly apparent in the BWSHG images as the FWSHG and BWSHG images converge in appearance. This observation suggests that there is an increase in the backscattered component of the FWSHG signal with increasing temperatures. This result is consistent with our observation that the specimen opacity tends to increase with increased thermal treatment. In order to quantify the extent of similarity between the FWSHG and BWSHG images, we computed an image correlation index (ICI) as defined in Eq. (2). The ICIs were computed for the FWSHG and BWSHG images at different temperatures, and the results are also plotted in Fig. 4. Below 60°C, ICIs on the corneal surface fluctuate between 0.17 and 0.27. However, the ICI value drastically increased from 0.22 at 55°C to 0.67 at 65°C. The image correlation analysis is consistent with the observation that the BWSHG images become increasingly similar to the FWSHG images at higher temperatures. In addition, normalized intensity of FWSHG, BWSHG, and MAF of the bovine corneal buttons at different temperatures are also shown in Fig. 4. Our results show a number of features associated with thermal treatment. First, MAF tends to increase with increasing temperatures, and there are local maxima of MAF at 50, 55, and 70°C, which correspond well with the peaks of the BWSHG. However, MAF drastically increases above 85°C. These observations

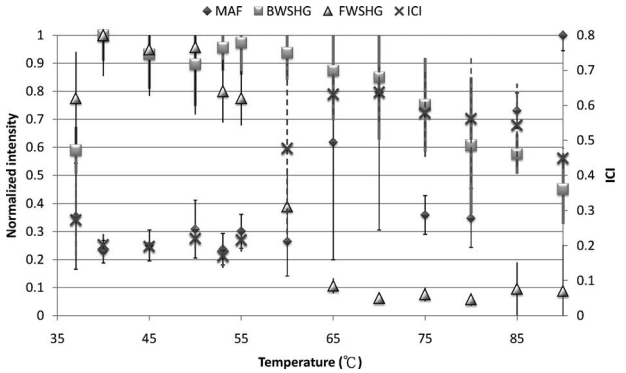

Fig. 4 Temperature dependence of ICI, normalized intensity of MAF, BWSHG, and FWSHG in thermally treated bovine corneal buttons at stromal surface.

suggest that at lower temperatures, MAF, most likely from the collagen cross-linkers, would modulate with changes in collagen organization. However, at higher temperatures, the formation of new autofluorescent species similar to the bityrosine molecules found under laser irradiation starts to appear.[31] In comparison, the FWSHG signal shows definitive decrease with increasing temperatures. Specifically, between 55 and 65°C, the relative FWSHG intensity changed from 0.78 to 0.11. The relative FWSHG intensity remained below 0.1 for all higher temperatures up to 90°C. The earlier study on porcine corneas indicated that the corneal thermal denaturation temperature is around 65°C,[14] and our qualitative image and FWSHG intensity results suggest that FWSHG is a more sensitive indicator of the extent of corneal thermal damage than the BWSHG signal.

4 Discussion

In this work, we used the multimodal imaging approach of multiphoton autofluorescence (MAF), forward second-harmonic generation (FWSHG), and backward second-harmonic generation (BWSHG) microscopy for characterizing the thermal denaturation of bovine corneal collagen. In addition to qualitative imaging, we quantitatively determined the temperature dependence of MAF, FWSHG, and BWSHG intensities. Furthermore, we attempted to correlate changes in FWSHG and BWSHG images by computing the image correlation index (ICI) at different temperatures. We found that MAF intensity has a general tendency to increase with temperature. The BWSHG increases when the temperature rises from 37 to 40°C, and as the treatment temperature increases, BWSHG shows a generally decreasing trend with local maximum at 55, 65, and 80°C. However, both the FWSHG and ICIs show a more drastic dependence on temperature, especially between 55 and 65°C. Specifically, FWSHG intensity decreased more than 80% within this temperature range, along with the appearance of the fibrous form of corneal collagen in the BWSHG images starting at 60°C. A reasonable explanation of BWSHG increasing from 37 to 40°C is that heat-induced collagen shrinkage increases the collagen density in tissue.[26,32,33]

After that, thermal damage causes denaturation when the temperature is higher than 60°C. We suggest that a combination of thermal effects in tissue and molecular level should be responsible for the thermal denaturation phenomenon. First, thermally induced reorganization of the collagen matrix in tissue level decreases FWSHG efficiency, which is highly related to fibril size, interfibril spacing, and fiber orientation.[34–36] Second, thermally induced tissue shrinkage increases localized collagen density, which may increase both FWSHG and BWSHG. The third mechanism is collagen denaturation at the molecular level, which reduces both FWSHG and BWSHG. Last, the increased tissue turbidity highly decreases FWSHG signals; however, it also contributes to backscattered signals. Moreover, the increase in backscattered signals also explains the increasing morphological similarity between FWSHG and BWSHG at higher temperatures.

In this work, we also repeat the experiment performed by Tan et al.,[12–14] obtaining the intensity profile of corneal BWSHG eyeballs. However, instead of porcine eyeballs, bovine eyeballs are used in our experiments. In addition, the heating

duration of eyeballs is elongated from 5 min to 10 min. Our results show similar trends as in the earlier study. However, the BWSHG intensity peaks are not that obvious and occur at different temperatures. The difference may originate from interspecies deviation and fundamental characteristics of collagen thermal denaturation. Some earlier reports suggest that partial renaturation related to hydration occurs during the heating process.[37,38] An experimental result based on differential scanning calorimetry shows that the thermally induced collagen phase transition in molecular level behaves like second-order phase transition.[39] Therefore, both duration and temperature of heating dominate the denaturation of collagen molecules. This phenomenon is also observed in a study of collagen denaturation performed on rat tail tendon.[27]

In conclusion, the combination of BWSHG, FWSHG, and MAF imaging and analysis may be used for the characterization of thermal damage in bovine corneas. With additional development, our approach may be extended to the clinical diagnosis of other corneal diseases.

Acknowledgments

We would like to acknowledge the support of the National Research Program for Genomic Medicine (NRPGM) of the National Science Council (NSC) in Taiwan for the support of this work. This project was completed at the Optical Molecular Imaging Microscopy Core Facility (A5) of NRPGM.

References

1. W. Denk, J. H. Strickler, and W. W. Webb, "2-photon laser scanning fluorescence microscopy," *Science* **248**(4951), 73–76 (1990).
2. S. J. Lin, R. J. Wu, H. Y. Tan, W. Lo, W. C. Lin, T. H. Young, C. J. Hsu, J. S. Chen, S. H. Jee, and C. Y. Dong, "Evaluating cutaneous photoaging by use of multiphoton fluorescence and second-harmonic generation microscopy," *Opt. Lett.* **30**(17), 2275–2277 (2005).
3. S. J. Lin, S. H. Jee, C. J. Kuo, R. J. Wu, W. C. Lin, J. S. Chen, Y. H. Liao, C. J. Hsu, T. F. Tsai, Y. F. Chen, and C. Y. Dong, "Discrimination of basal cell carcinoma from normal dermal stroma by quantitative multiphoton imaging," *Opt. Lett.* **31**(18), 2756–2758 (2006).
4. R. Cicchi, D. Massi, S. Sestini, P. Carli, V. De Giorgi, T. Lotti, and F. S. Pavone, "Multidimensional non-linear laser imaging of basal cell carcinoma," *Opt. Express* **15**(16), 10135–10148 (2007).
5. S. Q. Wang, A. W. Kopf, K. Koenig, D. Polsky, K. Nudel, and R. S. Bart, "Detection of melanomas in patients followed up with total cutaneous examinations, total cutaneous photography, and dermoscopy," *J. Am. Acad. Dermatol.* **50**(1), 15–20 (2004).
6. J. M. Houston, B. Adams, W. M. Petroll, H. D. Cavanagh, and J. V. Jester, "Corneal haze after excimer PTK in the mouse cornea related to stromal cell density and myofibroblast differentiation but not stromal growth," *Invest. Ophthalmol. Visual Sci.* **44**, U247–U247 (2003).
7. J. V. Jester, H. F. Li, W. M. Petroll, R. D. Parker, H. D. Cavanagh, G. J. Carr, B. Smith, and J. K. Maurer, "Area and depth of surfactant-induced corneal injury correlates with cell death," *Invest. Ophthalmol. Visual Sci.* **39**(6), 922–936 (1998).
8. T. Moller-Pedersen, H. D. Cavanagh, W. M. Petroll, and J. V. Jester, "Stromal wound healing explains refractive instability and haze development after photorefractive keratectomy—a 1-year confocal microscopic study," *Ophthalmology* **107**(7), 1235–1245 (2000).
9. T. Moller-Pedersen, H. F. Li, W. M. Petroll, H. D. Cavanagh, and J. V. Jester, "Confocal microscopic characterization of wound repair after photorefractive keratectomy," *Invest. Ophthalmol. Visual Sci.* **39**(3), 487–501 (1998).
10. T. Moller-Pedersen, M. Vogel, H. F. Li, W. M. Petroll, H. D. Cavanagh, and J. V. Jester, "Quantification of stromal thinning, epithelial thickness, and corneal haze after photorefractive keratectomy using *in vivo* confocal microscopy," *Ophthalmology* **104**(3), 360–368 (1997).
11. N. Morishige, A. J. Wahlert, M. C. Kenney, D. J. Brown, K. Kawamoto, T. Chikama, T. Nishida, and J. V. Jester, "Second-harmonic imaging microscopy of normal human and keratoconus cornea," *Invest. Ophthalmol. Visual Sci.* **48**(3), 1087–1094 (2007).
12. H. Y. Tan, Y. Sun, W. Lo, S. J. Lin, C. H. Hsiao, Y. F. Chen, S. C. M. Huang, W. C. Lin, S. H. Jee, H. S. Yu, and C. Y. Dong, "Multiphoton fluorescence and second harmonic generation imaging of the structural alterations in keratoconus *ex vivo*," *Invest. Ophthalmol. Visual Sci.* **47**(12), 5251–5259 (2006).
13. H. Y. Tan, Y. Sun, W. Lo, S. W. Teng, R. J. Wu, S. H. Jee, W. C. Lin, C. H. Hsiao, H. C. Lin, Y. F. Chen, D. H. K. Ma, S. C. M. Huang, S. J. Lin, and C. Y. Dong, "Multiphoton fluorescence and second harmonic generation microscopy for imaging infectious keratitis," *J. Biomed. Opt.* **12**(2), 024013 (2007).
14. H. Y. Tan, S. W. Teng, W. Lo, W. C. Lin, S. J. Lin, S. H. Jee, and C. Y. Dong, "Characterizing the thermally induced structural changes to intact porcine eye, part 1: second harmonic generation imaging of cornea stroma," *J. Biomed. Opt.* **10**(5), 054019 (2005).
15. B. G. Wang, K. Koenig, I. Riemann, R. Krieg, and K. J. Halbhuber, "Intraocular multiphoton microscopy with subcellular spatial resolution by infrared femtosecond lasers," *Histochem. Cell Biol.* **126**(4), 507–515 (2006).
16. W. Lo, S. W. Teng, H. Y. Tan, K. H. Kim, H. C. Chen, H. S. Lee, Y. F. Chen, P. T. C. So, and C. Y. Dong, "Intact corneal stroma visualization of GFP mouse revealed by multiphoton imaging," *Microsc. Res. Tech.* **69**(12), 973–975 (2006).
17. S. W. Teng, H. Y. Tan, J. L. Peng, H. H. Lin, K. H. Kim, W. Lo, Y. Sun, W. C. Lin, S. J. Lin, S. H. Jee, P. T. C. So, and C. Y. Dong, "Multiphoton autofluorescence and second-harmonic generation imaging of the *ex vivo* porcine eye," *Invest. Ophthalmol. Visual Sci.* **47**(3), 1216–1224 (2006).
18. S. W. Teng, H. Y. Tan, Y. Sun, S. J. Lin, W. Lo, C. M. Hsueh, C. H. Hsiao, W. C. Lin, S. C. M. Huang, and C. Y. Dong, "Multiphoton fluorescence and second-harmonic-generation microscopy for imaging structural alterations in corneal scar tissue in penetrating full-thickness wound," *Arch. Ophthalmol. (Chicago)* **125**(7), 977–978 (2007).
19. A. T. Yeh, N. Nassif, A. Zoumi, and B. J. Tromberg, "Selective corneal imaging using combined second-harmonic generation and two-photon excited fluorescence," *Opt. Lett.* **27**(23), 2082–2084 (2002).
20. T. J. Wang, W. Lo, C. M. Hsueh, M. S. Hsieh, F. R. Hu, and C. Y. Dong, "*Ex vivo* multiphoton analysis of rabbit corneal wound healing following conductive keratoplasty," *J. Biomed. Opt.* **13**(3), 034019 (2008).
21. M. Farid, N. Morishige, L. Lam, A. Wahlert, R. F. Steinert, and J. V. Jester, "Detection of corneal fibrosis by imaging second harmonic–generated signals in rabbit corneas treated with mitomycin C after excimer laser surface ablation," *Invest. Ophthalmol. Visual Sci.* **49**(10), 4377–4383 (2008).
22. D. J. Brown, N. Morishige, A. Neekhra, D. S. Minckler, and J. V. Jester, "Application of second harmonic imaging microscopy to assess structural changes in optic nerve head structure *ex vivo*," *J. Biomed. Opt.* **12**(2), 024029 (2007).
23. M. Han, G. Giese, and J. F. Bille, "Second harmonic generation imaging of collagen fibrils in cornea and sclera," *Opt. Express* **13**(15), 5791–5797 (2005).
24. F. Legare, C. Pfeffer, and B. R. Olsen, "The role of backscattering in SHG tissue imaging," *Biophys. J.* **93**(4), 1312–1320 (2007).
25. S. J. Lin, C. Y. Hsiao, Y. Sun, W. Lo, W. C. Lin, G. J. Jan, S. H. Jee, and C. Y. Dong, "Monitoring the thermally induced structural transitions of collagen by use of second-harmonic generation microscopy," *Opt. Lett.* **30**(6), 622–624 (2005).
26. S. J. Lin, W. Lo, H. Y. Tan, J. Y. Chan, W. L. Chen, S. H. Wang, Y. Sun, W. C. Lin, J. S. Chen, C. J. Hsu, J. W. Tjiu, H. S. Yu, S. H. Jee, and C. Y. Dong, "Prediction of heat-induced collagen shrinkage by use of second harmonic generation microscopy," *J. Biomed. Opt.* **11**(3), 034020 (2006).
27. Y. Sun, W. L. Chen, S. J. Lin, S. H. Jee, Y. F. Chen, L. C. Lin, P. T. C. So, and C. Y. Dong, "Investigating mechanisms of collagen thermal denaturation by high resolution second-harmonic generation imaging," *Biophys. J.* **91**(7), 2620–2625 (2006).
28. T. Theodossiou, G. S. Rapti, V. Hovhannisyan, E. Georgiou, K. Politopoulos, and D. Yova, "Thermally induced irreversible conformational changes in collagen probed by optical second harmonic gen-

eration and laser-induced fluorescence," *Lasers Med. Sci.* **17**(1), 34–41 (2002).
29. V. A. Hovhannisyan, W. Lo, C. Hu, S. J. Chen, and C. Y. Dong, "Dynamics of femtosecond laser photo-modification of collagen fibers," *Opt. Express* **16**(7), 7958–7968 (2008).
30. M. G. Lin, T. L. Yang, C. T. Chiang, H. C. Kao, J. N. Lee, W. Lo, S. H. Jee, Y. F. Chen, C. Y. Dong, and S. J. Lin, "Evaluation of dermal thermal damage by multiphoton autofluorescence and second-harmonic-generation microscopy," *J. Biomed. Opt.* **11**(6), 064006 2006).
31. M. Oujja, E. Rebollar, C. Abrusci, A. Del Amo, F. Catalina, and M. Castillejo, "UV, visible and IR laser interaction with gelatine," *J. Phys.: Conf. Ser.* **59**, 571–574 (2007).
32. C. E. Weir, "Rate of shrinkage of tendon collagen—heat, entropy, and free energy of activation of the shrinkage of untreated tendon. Effect of acid, salt, pickle, and tannage on the activation of tendon collagen," *J. Res. Natl. Bur. Stand.* **44**, 108–140 (1949).
33. K. Pankhurst, "Incipient shrinkage of collagen and gelatin," *Nature (London)* **159**(4042), 538–538 (1947).
34. R. M. Williams, W. R. Zipfel, and W. W. Webb, "Interpreting second-harmonic generation images of collagen I fibrils," *Biophys. J.* **88**(2), 1377–1386 (2005).
35. J. Mertz and L. Moreaux, "Second-harmonic generation by focused excitation of inhomogeneously distributed scatterers," *Opt. Commun.* **196**(1–6), 325–330 (2001).
36. L. Moreaux, O. Sandre, S. Charpak, M. Blanchard-Desce, and J. Mertz, "Coherent scattering in multi-harmonic light microscopy," *Biophys. J.* **80**(3), 1568–1574 (2001).
37. H. Hormann and H. Schlebus, "Reversible and irreversible denaturation of collagen fibers," *Biochemistry* **10**(6), 932–937 (1971).
38. M. Luescher, M. Ruegg, and P. Schindler, "Effect of hydration upon thermal-stability of tropocollagen and its dependence on presence of neutral salts," *Biopolymers* **13**(12), 2489–2503 (1974).
39. G. M. Mrevlishvili, N. O. Metreveli, G. Z. Razmadze, T. D. Mdzinarashvili, G. R. Kakabadze, and M. M. Khvedelidze, "Partial heat capacity change—fundamental characteristic of the process of thermal denaturation of biological macromolecules (proteins and nucleic acids)," *Thermochim. Acta* **308**(1–2), 41–48 (1998).